Journal of Applied Mathematics and Physics, 2025, 13(3), 914-932
https://www.scirp.org/journal/jamp
ISSN Online: 2327-4379
ISSN Print: 2327-4352

Numerical Simulation Analysis of Large-Scale Three-Dimensional Planting Greenhouse Based on Orthogonal Test Method

Hao Cai[1], Zhen Liang[2], Yingying Lyu[3], Yinuo Qin[1]

[1]College of Environmental Science and Engineering, Donghua University, Shanghai, China
[2]Institute of Heating, Ventilation and Air Conditioning, Donghua University, Shanghai, China
[3]School of Civil Engineering, Chongqing University, Chongqing, China
Email: 2232482@gmail.dhu.edu.cn, liangzhen@dhu.edu.cn

How to cite this paper: Cai, H., Liang, Z., Lyu, Y.Y. and Qin, Y.N. (2025) Numerical Simulation Analysis of Large-Scale Three-Dimensional Planting Greenhouse Based on Orthogonal Test Method. *Journal of Applied Mathematics and Physics*, **13**, 914-932.
https://doi.org/10.4236/jamp.2025.133048

Received: February 19, 2025
Accepted: March 22, 2025
Published: March 25, 2025

Abstract

Maintaining optimal indoor environmental conditions for plant growth in greenhouse structures during hot summer periods presents a significant challenge in many regions. While natural and mechanical ventilation methods are commonly employed, there is a notable lack of theoretical simulation studies on greenhouse ventilation, particularly those incorporating light radiation and plant transpiration effects. This study employs Computational Fluid Dynamics (CFD) to simulate greenhouse environments, uniquely integrating both light radiation and plant transpiration factors in the analysis of mechanical ventilation characteristics. Through a combination of transient and steady-state calculations, temperature and humidity fields were comprehensively analyzed. Results indicate that positive pressure ventilation, symmetrical fan arrangement, and longitudinal airflow across plant shelves yield superior performance. Utilizing orthogonal experimental design and range analysis methodologies, a multi-factor variable analysis was conducted. Findings reveal that fan velocity exerts the most significant influence on the temperature field and the theoretical optimal combination was tested, and the most suitable combination scheme is selected according to the simulation results. This research provides valuable theoretical guidance for temperature and humidity control in greenhouses situated in subtropical monsoon climates.

Keywords

Greenhouse, Air Distribution, Spray Cooling, Numerical Simulation, Mechanical Ventilation, CFD

1. Introduction

1.1. Large-Scale Solar Greenhouse

Agricultural greenhouse systems play a crucial role in modern agriculture, significantly enhancing crop growth, yield, and annual production stability. In the context of global climate change and population growth, in-depth research on temperature and humidity control in greenhouse systems is fundamental to achieving precision agriculture and driving the development of more efficient, environmentally friendly, and sustainable modern agricultural practices.

Recent trends in advanced greenhouse design globally have been towards larger-scale structures [1]. These large-scale greenhouses provide controlled environments where temperature, humidity, light, and CO_2 concentration can be artificially or automatically regulated to create optimal growth conditions. The regulation of the greenhouse air environment is an important factor in ensuring healthy crop growth, and is centered on the precise control of air temperature, humidity, CO_2 concentration and other parameters [2]. However, due to longwave radiation effects, greenhouse temperatures often exceed 40˚C [3], particularly in summer, presenting significant cooling challenges.

Heat exchange in greenhouses primarily occurs through radiation, convection, and conduction [4] [5], while water exchange involves evaporation and condensation processes. Recent studies have explored innovative approaches to manage these environmental factors. For instance, Bai *et al.* [6] investigated the effects of forced soil aeration at different depths on tomato root systems and growth environments using PVC pipes installed at 20 cm and 30 cm depths in tomato cultivation areas. Han *et al.* [7] examined the impact of varying rhizosphere temperatures on tomato leaf stomata, revealing that increased root zone temperatures led to reduced stomatal size and aperture but increased stomatal density, a response mechanism to high-temperature stress.

1.2. Vertical Farming Techniques

Vertical farming techniques, which utilize vertical space to cultivate different crops simultaneously, have shown promise in improving greenhouse land use efficiency. Studies by Yue *et al.* [8] and Li *et al.* [9] demonstrated significant economic benefits through increased planting efficiency in greenhouses using vertical farming methods.

1.3. CFD in Greenhouse

Computational Fluid Dynamics (CFD), an evolution of Computer-Aided Engineering (CAE) technologies, has emerged as a powerful tool in greenhouse design and optimization. By solving equations for mass, momentum, and energy conservation, CFD can predict fluid flow, heat and mass transfer, chemical reactions, and other related phenomena. Since Okushima *et al.* [10] pioneered the application of Computational Fluid Dynamics (CFD) to greenhouse environments in 1989, this technology has become indispensable for simulating temperature and

humidity fields, thereby enhancing the precision of internal environmental control in greenhouse agriculture. The evolution of CFD applications in this domain reflects the ongoing pursuit of energy-efficient and sustainable agricultural practices, a central theme in energy and environment research. Molina-Aiz *et al.* [11] conducted a comparative study of finite element and control volume discretization methods for greenhouse ventilation simulation. Their analysis of accuracy and computational efficiency in incompressible turbulent flow revealed comparable high precision for both methods, with finite element methods requiring more computational resources. This research underscores the importance of optimizing numerical methods for energy-efficient greenhouse design and operation. Kang *et al.* [12] highlighted that the use of first-order upwind schemes in greenhouse numerical simulations results in significant discrepancies when compared to experimental data. Therefore a second or higher order windward format is required in CFD. Saberian *et al.* [13] demonstrated through CFD simulations that fan-assisted natural ventilation systems can effectively reduce the internal temperature of greenhouses during the summer. Xu *et al.* [14] used the SST turbulence model in their simulations, discovering that fan power density significantly influenced the cooling performance of the PFC system in greenhouses. Stefano Benni *et al.* [15] investigated various ventilation configurations, demonstrating that closing windward roof vents while maintaining open side vents yielded optimal cooling effects. Xu *et al.* [16] employed solar ray tracing methods to simulate temperature and velocity fields within greenhouses, optimizing parameters such as greenhouse length, wet curtain area, and fan speed. Shao *et al.* [17] utilized CFD to determine optimal ventilation port locations and sizes, as well as ideal configurations for wet curtain fans, achieving optimal temperature control. He *et al.* [18] developed a two-dimensional transient CFD simulation model to simulate air temperature in greenhouses with movable back walls, revealing an average temperature reduction of about 1.7˚C compared to traditional brick wall greenhouses. Xin Zhang *et al.* [19] integrated CFD modeling with multi-criteria optimization to enhance solar greenhouse design and performance, balancing thermal environment, energy efficiency, and economic factors. This holistic approach addresses the complex interplay between energy use, environmental control, and economic viability in agricultural systems. Villagran *et al.* [20] employed CFD to study natural ventilation in three different greenhouse types under tropical mountain climates. This research contributes to our understanding of passive climate control strategies in diverse geographical contexts, a crucial aspect of developing energy-efficient agricultural practices globally. J.C. Roy [21] highlighted the critical role of plant transpiration in greenhouse environment management. This observation underscores the importance of biophysical processes in energy-efficient climate control, emphasizing the need for integrated approaches that consider both technological and biological factors in greenhouse design and operation. These studies collectively demonstrate the evolving sophistication of CFD applications in greenhouse agriculture, reflecting a growing emphasis on energy efficiency, sustainability, and

holistic system optimization.

2. Model Design and Validation

2.1. Physical Model

This study employs the widely-used commercial software Fluent to simulate physical fields using the control volume method [22]. Physical modeling was conducted using Space Claim, with fluid domains extracted for analysis. The multi-span greenhouse model features a base area of 16 m × 16 m, a ridge height of 3 m, and an arched roof peak at 5 m. The interior contains two rows of 15 columns of vertical planting aluminum racks, with 0.2 m thick plant cultivation zones at heights of 0.5 m and 1.2 m (Figure 1 and Figure 2).

To simulate the transpiration of plants, some surfaces are designated as discrete phase inlets, constantly releasing small droplets outward. Four aluminum rack surfaces are set as inlets to model CO_2 release from gas fertilization. Mechanical ventilation is simulated by two fans on each side of the greenhouse, with roof vents serving as outlets. For cooling purposes, 4 × 7 misting nozzles are positioned above the plant zones (Figure 3). Table 1 shows the physical property parameters of different materials.

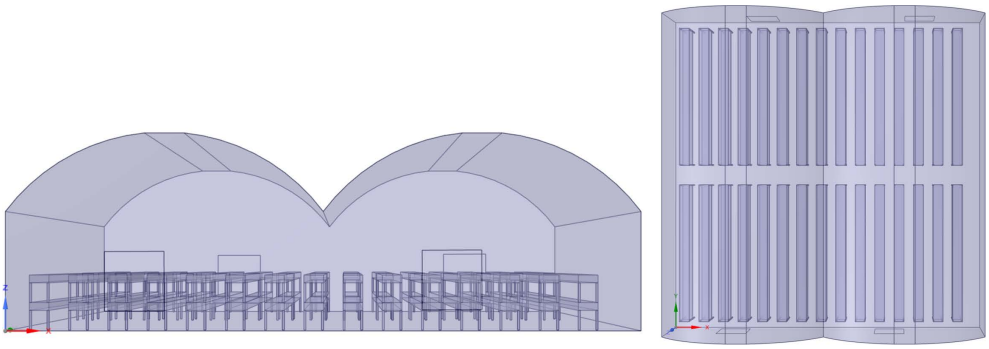

Figure 1. Physical model of greenhouse.

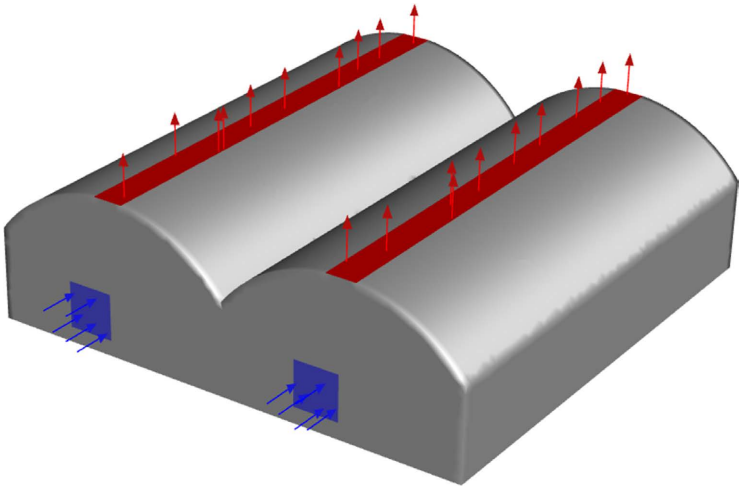

Figure 2. Greenhouse inlet and outlet.

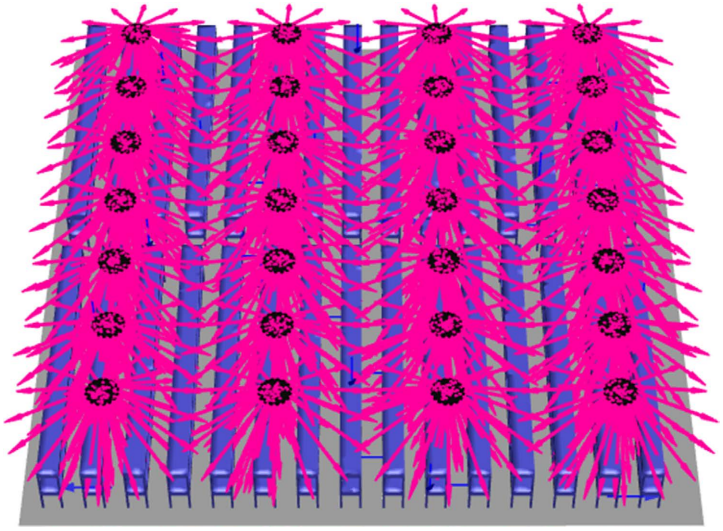

Figure 3. Sprinkler position.

Table 1. Material property parameters.

Material	Density/ ($kg \cdot m^{-3}$)	Specific heat capacity/ ($J \cdot kg^{-1} \cdot K^{-1}$)	Thermal conductivity /($W \cdot m^{-1} \cdot K^{-1}$)	Absorption coefficient	Scattering coefficient	Index of refraction
N_2	1.138	segmentation function	0.0242	0	0	1
O_2	1.2999	segmentation function	0.0246	0	0	1
CO_2	1.7878	segmentation function	0.0145	0.43	0	1
Vapor	0.5542	segmentation function	0.0261	0.54	0	1
Plastics	1380	900	0.1596	0.1	0	0.9
Soil	1900	2200	2	0.5	1	0.9
Al	2719	871	202.4	0	0	1

2.2. Boundary Conditions

Table 2 shows the inlet and outlet boundary condition settings, with the fan blowing positive pressure ventilation and wind speed of 2 $m \cdot s^{-1}$ as an example.

2.3. Solver Selections

The simulation utilizes a pressure-based solver in Fluent, as no significant density variations are anticipated. A combination of transient and steady-state methods is employed to observe flow fields for various pressure scenarios, while only steady-state analysis is used for multi-factor simulations using orthogonal experimental design.

The Realizable k-ε turbulence model is adopted, having been effectively applied

Table 2. Boundary condition settings.

Boundary	Type	Parameterization
Wall-soil	Wall	temp: 35˚C DPM type: trap
Wall-plastic	Wall	heat transfer coefficient: 20.256 $W \cdot m^{-2} \cdot K^{-1}$ incoming temperature: 38.5˚C Radiation BC type: translucent DPM type: reflect
Wall-plants	Wall	temp: 35˚C DPM type: trap
Wall-Al	Wall	temp: 30˚C DPM type: reflect
Outlet	Pressure-outlet	gauge pressure: 0 Pa reflux inhibition DPM type: escape
Inlet-fan	velocity-inlet	velocity: 2 $m \cdot s^{-1}$ temp: 38.5˚C species: H_2O, O_2, CO_2, N_2 DPM type: escape
Inlet-CO_2	Mass-flow-inlet	flow rate: 0.00005 $kg \cdot s^{-1}$ temp: 25˚C species: CO_2, O_2 DPM type: reflect

in various flow simulations [23]. Turbulence model constants are set as follows: C2-Epsilon = 1.9, TKE Prandtl number = 1, TDR Prandtl number = 1.2, Energy Prandtl number = 0.85, Wall Prandtl number = 0.85, and Turbulent Schmidt number = 0.7.

Based on the model's dimensionless y^+ value (**Figure 4**: average 68), the Menter-Lechner near-wall model is selected [24] [25], which automatically adapts turbulence laws according to y^+ values.

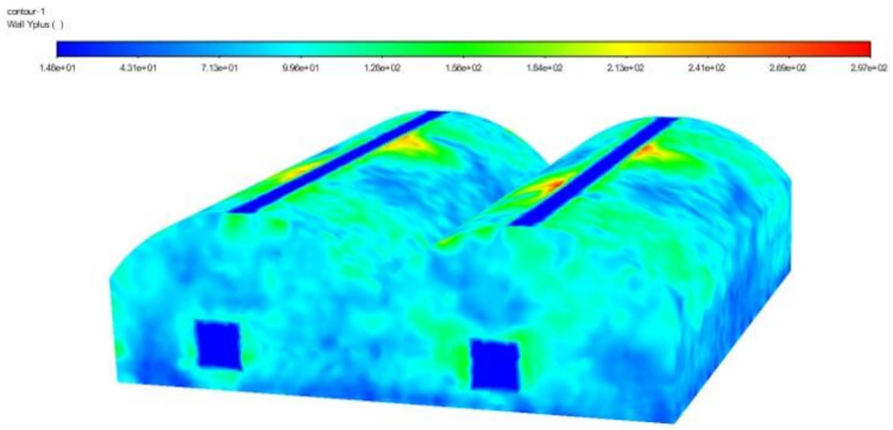

Figure 4. y^+ value distribution.

A species transport model was employed to monitor relative humidity variations, with diffusion energy source, complete multi-component diffusion, and thermal diffusion activated. Given the low liquid droplet content in the flow field (well below 10%), the Discrete Phase Model (DPM) was utilized to simulate mist cooling, incorporating convection/diffusion control, thermophoretic force, and temperature-dependent latent heat. Table 3 shows the DPM discrete phase setup parameters.

For steady-state calculations, a Coupled pressure-based solver was used, while the PISO solver was employed for transient simulations. The Green-Gauss Node-Based method was selected for gradient discretization, with PRESTO for pressure interpolation. Due to the complexity of the activated equation models, the Third-order MUSCL scheme was chosen for both convection terms and discrete phase calculations.

Table 3. DPM setting parameters.

	Nozzle type	Caliber [26] /(mm)	Temp /(˚C)	Direction	Velocity /(m·s^{-1})	Cone angle /(˚)	Flow rate /(kg·s^{-1})
Droplet	solid-cone	0.01	18	Z=-1	26.8	60	0.002
Plant Transpiration	surface	0.001	35	-	0.1	-	0.002025 [27]

2.4. Assumptions

To simplify computations, the following assumptions were made: 1) local unidirectionality at numerical outlets; 2) negligible droplet collision and breakup; 3) Boussinesq approximation for fluid dynamics [28]; 4) The transpiration rate is influenced dynamically by temperature, humidity, light intensity, and other factors. This simulation primarily focused on the humidity changes over a 220-second period, which is relatively short, and as such, the biological changes during this time are slow. Additionally, we applied a higher transpiration rate, as presented in Reference [27], which significantly affects the humidity. If humidity can be controlled under this scenario, other conditions should not pose any issues. So we neglect the rate of change of plant photosynthesis and transpiration with time and temperature. Taking the values of the experimental group of CK Xiangyun chrysanthemum flowers with normal water supply by Kong *et al.* [27]; 5) Carbon dioxide gas fertilizer tends to be stored in liquid form below −30˚C, so the temperature at which it is released is low, and the release temperature is set at 25˚C, taking into account the cooling effect and the plant's suitability for the temperature.

2.5. Grid Segmentation and Irrelevance Verification

Mesh generation was performed using Workbench Meshing, primarily employing tetrahedral elements with a base size of 250 mm, curvature capture of 80 mm, and proximity capture of 150 mm. Mesh refinement was applied near plant areas. The

resulting mesh comprised 1,255,393 elements (Figure 5), with an average skewness of 0.23 (maximum 0.77) and an average orthogonal quality of 0.77 (minimum 0.23), indicating suitable quality for simulation purposes.

Figure 5. Mesh generation.

A refined computational mesh enables more accurate resolution of small-scale phenomena in fluid dynamics, such as near-wall flows or complex flow patterns around equipment. However, increasing mesh density necessitates greater computational resources and time. Therefore, it is imperative to optimize the mesh while maintaining simulation accuracy, thereby minimizing unnecessary computational burden. Local mesh refinement strategies can be employed in critical areas such as ventilation outlets, heating elements, and vegetation zones to precisely capture flow and temperature field variations. This approach enhances accuracy in these key regions without significantly increasing overall computational load. To ensure mesh-independent results, a grid sensitivity analysis was conducted. As illustrated in Figure 6, temperature variations at five monitoring points were minimal with increasing mesh refinement, indicating that the simulation outcomes are not significantly influenced by mesh size beyond a certain resolution.

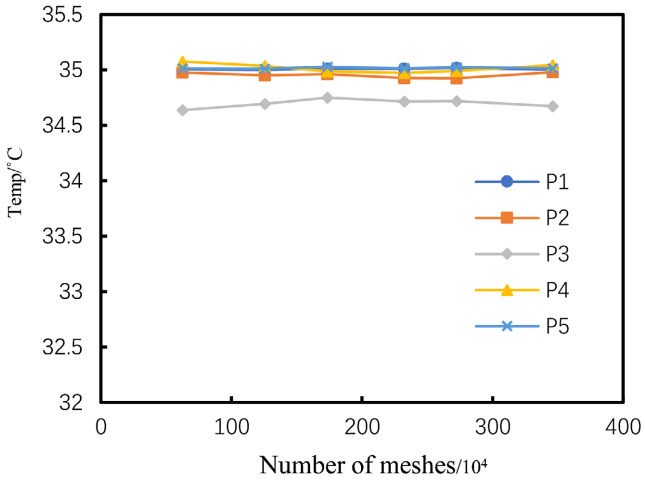

Figure 6. Variation of temperature measurement points with the number of meshes.

2.6. Model Validation

The simulation results were validated against experimental data from the Shanghai Academy of Agricultural Sciences (August 2022) [29]. The maximum temperature discrepancy was −5.3% at point P2 (**Figure 7**), while the maximum humidity discrepancy was 6.96% at point P4 (**Figure 8**). During the development of the greenhouse model in Fluent, certain complex physical processes may have been simplified or assumed. For example, the small airflows within the greenhouse structure, the impact of gaps in windows and doors on the temperature and humidity distribution, or the assumption of ideal boundary conditions, which may not fully reflect the real-world conditions. Additionally, some physical parameters within the greenhouse, such as droplet diameter and spray outlet speed, might differ slightly from the actual experiment. In the Fluent solution process, numerical methods may also introduce minor errors, such as those related to discretization schemes and convergence precision. However, the maximum error observed was only 7%, with most errors staying within 5%, which is within a reasonable range for simulation accuracy.

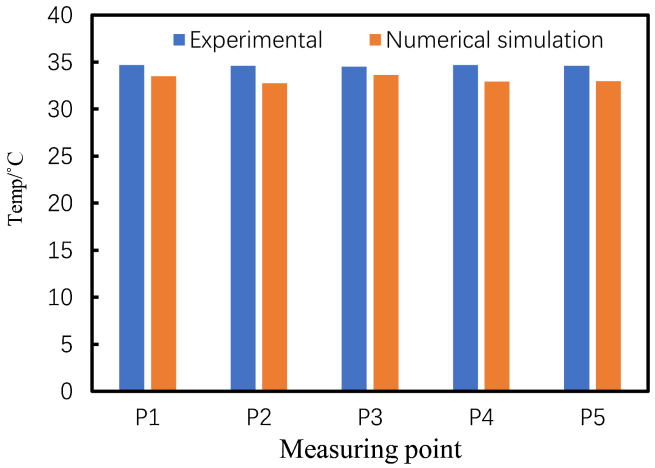

Figure 7. Comparison of measured and simulated temperatures at points.

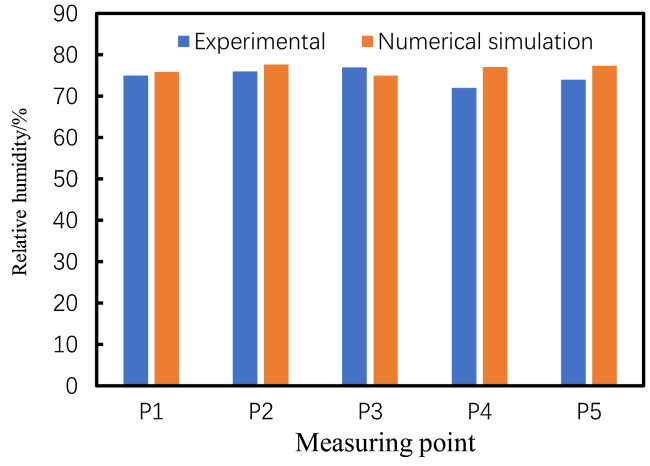

Figure 8. Comparison of measured and simulated humidity at points.

3. Simulation Results and Discussion

3.1. Ventilation Methods

This study simulated greenhouse conditions based on outdoor meteorological data from the Shanghai Academy of Agricultural Sciences (August 2022), assuming an initial indoor temperature of 40˚C prior to mist cooling activation. The simulation compared positive and negative pressure ventilation systems under mist cooling conditions (Figure 9).

Results indicate that (Figure 10) both ventilation systems led to temperature

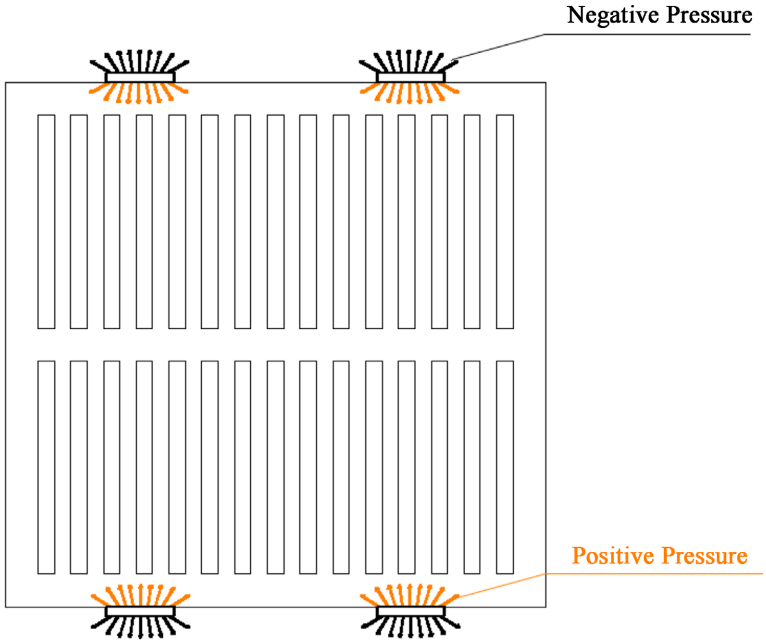

Figure 9. Ventilation methods.

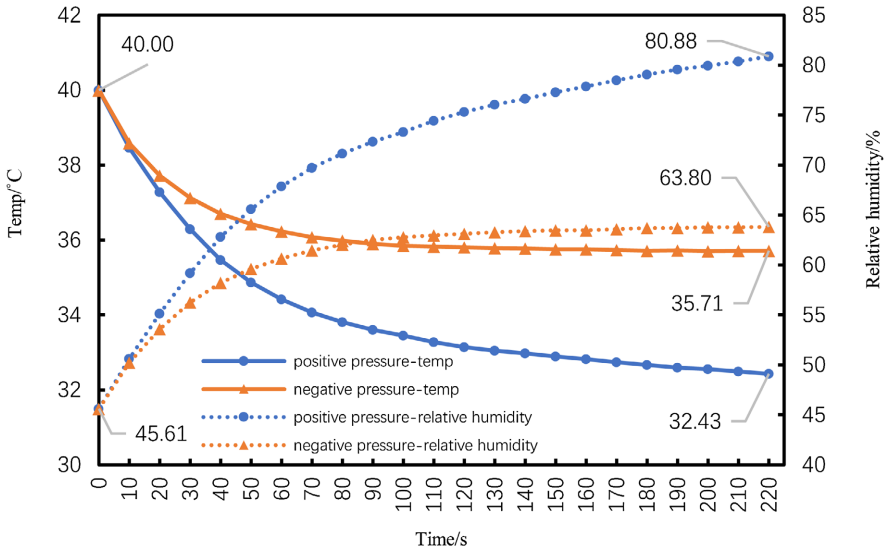

Figure 10. Average temperature and humidity in the greenhouse during positive/negative fan ventilation.

decreases and humidity increases upon mist activation. After 10 seconds, significant differences emerged between the two systems. The positive pressure system demonstrated more rapid temperature reduction and humidity increase, likely due to its airflow pattern aligning with natural thermal buoyancy, unlike the negative pressure system's opposing flow direction.

Both systems exhibited rapid cooling in the first 40 seconds, with rates decreasing thereafter until stabilization at 220 seconds. At this point, the positive pressure system achieved a temperature 3.28˚C lower than the negative pressure system, indicating superior cooling efficiency. Steady-state simulations revealed average temperatures and humidities of 32.81˚C and 78.89% for the positive pressure system, compared to 35.17˚C and 68.52% for the negative pressure system. Considering that chrysanthemums grow well below 90% relative humidity and are more sensitive to temperature variations, the positive pressure system was selected for further investigation.

3.2. Fan Arrangement

Subsequent simulations compared symmetrical and interleaved fan arrangements under identical initial conditions (Figure 11).

Both arrangements showed similar temperature reductions (approximately 2˚C) and humidity increases in the first 40 seconds (Figure 12). The temperature drop changed after 50 s. The temperature drop was slightly faster in the symmetrical arrangement than in the interleaved arrangement. The slightly faster temperature drops in the symmetrical arrangement than in the interleaved arrangement may be due to the collision of the symmetrical fan airflow on both sides after reaching the middle of the greenhouse, which spreads laterally and accelerates the indoor gas perturbation. The gasification rate of the spray was made faster, and more heat was taken away, resulting in a lower temperature. However, between 130 - 220 seconds, the interleaved arrangement achieved marginally

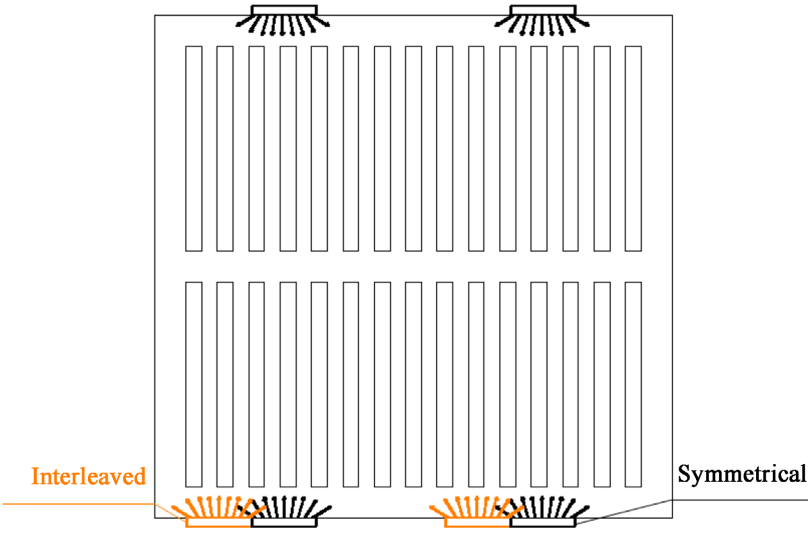

Figure 11. Fan arrangement.

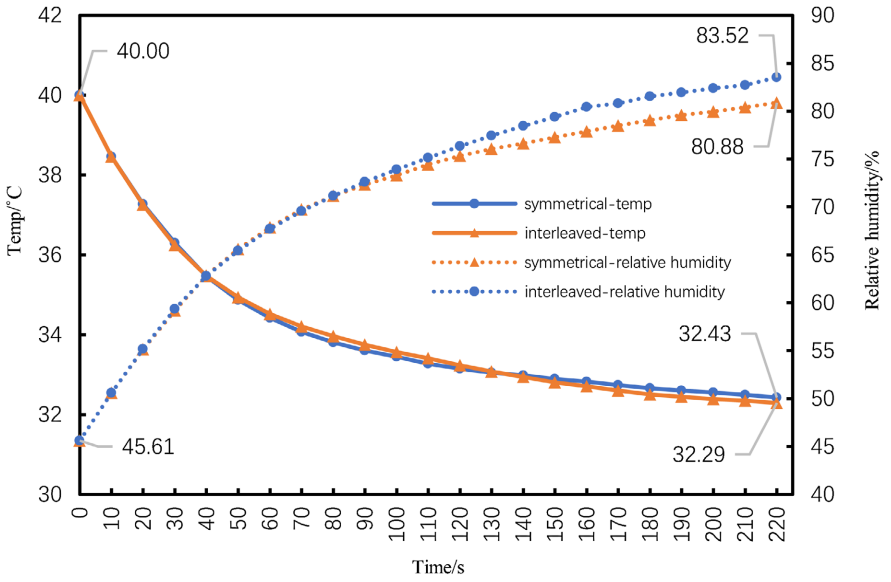

Figure 12. Average temperature and humidity in the greenhouse with symmetrical/interleaved fan arrangement.

lower temperatures (by about 0.15˚C) but with 3% higher humidity.

Steady-state simulations yielded average temperatures and humidities of 32.81˚C and 78.89% for the symmetrical arrangement, and 32.86˚C and 80.53% for the interleaved arrangement. Given the larger difference in humidity compared to temperature, and to mitigate potential high-humidity risks, the symmetrical fan arrangement was ultimately selected as the optimal configuration.

3.3. Fan Air Output Mode

This study investigated the impact of fan orientation on greenhouse microclimate, comparing longitudinal and transverse airflow patterns relative to plant shelves (**Figure 13**). Simulations were conducted under identical initial and boundary conditions to isolate the effects of airflow direction.

The results demonstrate that both orientations exhibited similar temperature and humidity trends during the initial 40 seconds of operation (**Figure 14**). However, significant divergence emerged after 60 seconds. The longitudinal airflow configuration demonstrated markedly faster temperature reduction, consistently maintaining temperatures approximately 0.6˚C lower than the transverse configuration between 120 - 220 seconds, before stabilizing.

Conversely, the longitudinal configuration resulted in higher relative humidity levels, increasing more rapidly and reaching 3.8% higher than the transverse configuration at 220 seconds. Steady-state simulations revealed average temperature and humidity values of 32.81˚C and 78.89% for the longitudinal configuration, compared to 33.12˚C and 76.85% for the transverse configuration.

Considering that chrysanthemums can thrive at relative humidity levels below 90% and are more sensitive to temperature variations than humidity fluctuations, the longitudinal airflow configuration was deemed optimal for this greenhouse application.

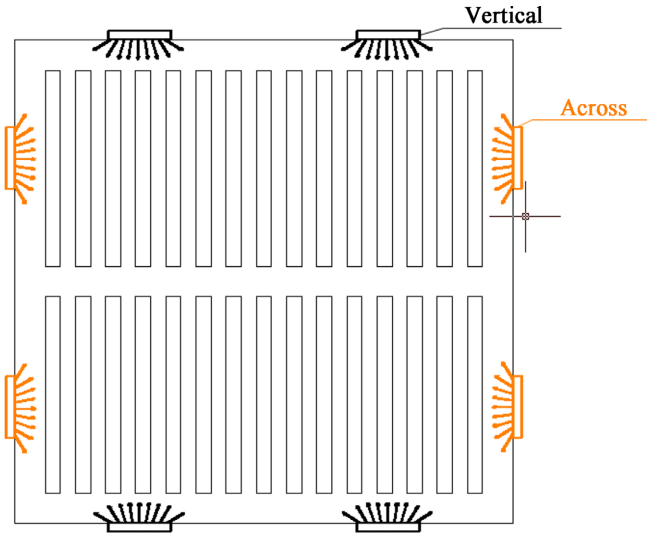

Figure 13. Fan air output mode.

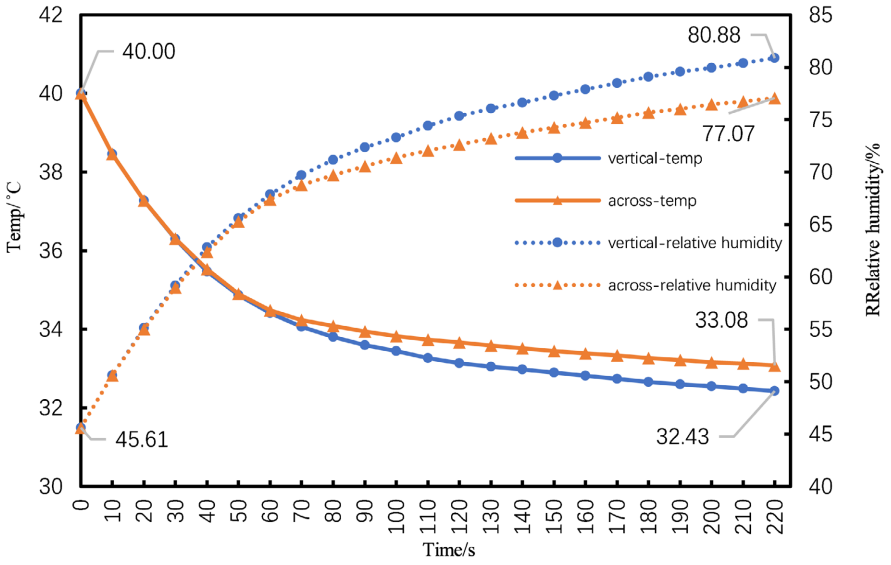

Figure 14. Average temperature and humidity in the greenhouse with fans blowing vertically/horizontally across the plant stand.

3.4. Orthogonal Tests and Analysis of Variance

Building upon previous findings, this study employed a multi-factorial optimization approach to investigate the combined effects of fan height, air velocity, misting nozzle height, and misting flow rate on greenhouse microclimate. To efficiently explore this complex parameter space, which would require 625 individual experiments if fully explored, an orthogonal experimental design was implemented.

The orthogonal design method, widely recognized for its ability to yield reliable and representative results with reduced experimental iterations, was utilized to identify optimal combinations of these four critical factors, each evaluated at five levels. This approach not only minimizes resource consumption and time require-

ments but also enables the extraction of statistically significant insights from a limited number of experimental runs [30].

Table 4 presents the orthogonal design matrix for the four factors at five levels. The primary optimization criterion [31] was set to achieve an average temperature closest to 20˚C [32], which is considered optimal for chrysanthemum growth. Temperature measurements were averaged across two horizontal planes within the plant zone (z = 0.6 m and z = 1.3 m). A secondary constraint of maintaining relative humidity below 90% was imposed to prevent potential moisture-related issues.

Table 5 presents the simulated temperature and humidity data for 25 experimental configurations derived from the orthogonal array design. Initial analysis identified configuration 17 as yielding the lowest temperature (30.21˚C). However, a more comprehensive range analysis revealed fan velocity as the most influential factor and suggested an optimal parameter combination of $A_5B_1C_1D_4$ (not included in the initial experimental set).

Table 4. Different factors and variables.

Fan height /(m)	Fan flow rate /(m·s^{-1})	Nozzle height /(m)	Spray flow rate /(kg·s^{-1})
0.5	1	2	0.0015
1	1.5	2.5	0.002
1.5	2	3	0.0025
2	2.5	3.5	0.003
2.5	3	4	0.0035

Table 5. Orthogonal extreme variance analysis table.

No.	A: Fan height /(m)	B: Fan velocity /(m·s^{-1})	C: Nozzle height /(m)	D: Spray flow rate /(kg·s^{-1})	Test index: temp /(˚C)
1	0.5	1	2	0.0015	x_1 = 30.82
2	0.5	1.5	3	0.003	x_2 = 31.13
3	0.5	2	4	0.002	x_3 = 33.16
4	0.5	2.5	2.5	0.0035	x_4 = 33.26
5	0.5	3	3.5	0.0025	x_5 = 34.98
6	1	1	4	0.003	x_6 = 30.72
7	1	1.5	2.5	0.002	x_7 = 30.83
8	1	2	3.5	0.0035	x_8 = 30.99
9	1	2.5	2	0.0025	x_9 = 32.34
10	1	3	3	0.0015	x_{10} = 35.50
11	1.5	1	3.5	0.002	x_{11} = 30.32
12	1.5	1.5	2	0.0035	x_{12} = 30.30

Continued

13	1.5	2	3	0.0025	$x_{13} = 31.16$
14	1.5	2.5	4	0.0015	$x_{14} = 34.82$
15	1.5	3	2.5	0.003	$x_{15} = 32.59$
16	2	1	3	0.0035	$x_{16} = 30.42$
17	2	1.5	4	0.0025	$x_{17} = 30.21$
18	2	2	2.5	0.0015	$x_{18} = 31.53$
19	2	2.5	3.5	0.003	$x_{19} = 31.43$
20	2	3	2	0.002	$x_{20} = 33.53$
21	2.5	1	2.5	0.0025	$x_{21} = 30.40$
22	2.5	1.5	3.5	0.0015	$x_{22} = 30.39$
23	2.5	2	2	0.003	$x_{23} = 30.76$
24	2.5	2.5	3	0.002	$x_{24} = 31.91$
25	2.5	3	4	0.0035	$x_{25} = 31.92$
T_{l1}	$T_{A1} = x_1 + x_2 + x_3 + x_4 + x_5 = 163.35$	$T_{B1} = x_1 + x_6 + x_{11} + x_{16} + x_{21} = 152.68$	$T_{C1} = x_1 + x_9 + x_{12} + x_{20} + x_{23} = 157.75$	$T_{D1} = x_1 + x_{10} + x_{14} + x_{18} + x_{22} = 163.06$	
T_{l2}	$T_{A2} = x_6 + x_7 + x_8 + x_9 + x_{10} = 160.38$	$T_{B2} = x_2 + x_7 + x_{12} + x_{17} + x_{22} = 152.86$	$T_{C2} = x_4 + x_7 + x_{15} + x_{18} + x_{21} = 158.61$	$T_{D2} = x_3 + x_7 + x_{11} + x_{20} + x_{24} = 159.75$	
T_{l3}	$T_{A3} = x_{11} + x_{12} + x_{13} + x_{14} + x_{15} = 159.19$	$T_{B3} = x_3 + x_8 + x_{13} + x_{18} + x_{23} = 157.60$	$T_{C3} = x_2 + x_{10} + x_{13} + x_{16} + x_{24} = 160.12$	$T_{D3} = x_5 + x_9 + x_{13} + x_{17} + x_{21} = 159.09$	
T_{l4}	$T_{A4} = x_{16} + x_{17} + x_{18} + x_{19} + x_{20} = 157.12$	$T_{B4} = x_4 + x_9 + x_{14} + x_{19} + x_{24} = 163.76$	$T_{C4} = x_5 + x_8 + x_{11} + x_{19} + x_{22} = 158.11$	$T_{D4} = x_2 + x_6 + x_{15} + x_{19} + x_{23} = 156.63$	
T_{l5}	$T_{A5} = x_{21} + x_{22} + x_{23} + x_{24} + x_{25} = 155.38$	$T_{B5} = x_5 + x_{10} + x_{15} + x_{20} + x_{25} = 168.52$	$T_{C5} = x_3 + x_6 + x_{14} + x_{17} + x_{25} = 160.83$	$T_{D5} = x_4 + x_8 + x_{12} + x_{16} + x_{25} = 156.89$	$T = \sum_{i=1}^{25} x_i$
K_{l1}	$K_{A1} = T_{A1}/5 = 32.67$	$K_{B1} = T_{B1}/5 = 30.54$	$K_{C1} = T_{C1}/5 = 31.55$	$K_{D1} = T_{D1}/5 = 32.61$	
K_{l2}	$K_{A2} = T_{A2}/5 = 32.08$	$K_{B2} = T_{B2}/5 = 30.57$	$K_{C2} = T_{C2}/5 = 31.72$	$K_{D2} = T_{D2}/5 = 31.95$	
K_{l3}	$K_{A3} = T_{A3}/5 = 31.84$	$K_{B3} = T_{B3}/5 = 31.52$	$K_{C3} = T_{C3}/5 = 32.02$	$K_{D3} = T_{D3}/5 = 31.82$	
K_{l4}	$K_{A4} = T_{A4}/5 = 31.42$	$K_{B4} = T_{B4}/5 = 32.75$	$K_{C4} = T_{C4}/5 = 31.62$	$K_{D4} = T_{D4}/5 = 31.33$	
K_{l5}	$K_{A5} = T_{A5}/5 = 31.08$	$K_{B5} = T_{B5}/5 = 33.70$	$K_{C5} = T_{C5}/5 = 32.17$	$K_{D5} = T_{D5}/5 = 31.38$	
ΔK	$\Delta K_A = 1.59$	$\Delta K_B = 3.16$	$\Delta K_C = 0.62$	$\Delta K_D = 1.28$	

Subsequent simulation of this derived optimal configuration yielded an average temperature of 30.71˚C. However, the associated relative humidity reached 100%, rendering this configuration unsuitable for plant growth despite its temperature advantages. This finding underscores the critical importance of considering multiple environmental parameters in greenhouse climate optimization.

Balancing both temperature and humidity considerations, configuration 24 was ultimately selected as the optimal solution. This configuration, characterized by a fan height of 2.5 m, fan velocity of 2.5 m·s^{-1}, misting nozzle height of 3 m, and

misting flow rate of 0.002 $kg \cdot s^{-1}$, resulted in an average temperature of 31.91˚C and relative humidity of 85.14%.

4. Conclusions

In summary, this work employed advanced Computational Fluid Dynamics (CFD) techniques to optimize the microclimate in large-scale multi-span greenhouses, focusing on temperature and humidity control. The findings underscore the importance of considering multiple environmental parameters simultaneously when optimizing greenhouse climate control. While lower temperatures might initially seem preferable, associated high humidity levels can render such conditions suboptimal for plant growth. This nuanced approach to environmental control can lead to more energy-efficient greenhouse operations by avoiding over-cooling or excessive dehumidification.

Transient and steady-state simulations were conducted to evaluate individual factors. Prioritizing cooling efficiency, the study identified positive pressure ventilation, symmetrical fan arrangement, and longitudinal airflow relative to plant shelves as optimal configurations, achieving lower average temperatures while maintaining humidity within the acceptable range for plant growth.

An orthogonal experimental design was implemented to analyze the complex interactions between four key factors: fan height, fan velocity, misting nozzle height, and misting flow rate. Each factor was evaluated at five levels. Range analysis revealed fan velocity as the most influential factor on temperature distribution. While the theoretical optimal combination derived from range analysis yielded an average temperature of 30.71˚C, it was discarded due to 100% relative humidity, which would severely impact plant growth. Balancing temperature and humidity considerations, the study ultimately selected configuration 24 (fan height: 2.5 m, fan velocity: 2.5 $m \cdot s^{-1}$, nozzle height: 3 m, misting flow rate: 0.002 $kg \cdot s^{-1}$), resulting in an average temperature of 31.91˚C and relative humidity of 85.14%.

The optimized configuration identified in this study offers a balanced solution for chrysanthemum cultivation, potentially improving energy efficiency while maintaining suitable growing conditions. Based on the optimal combination identified through the orthogonal experiment, it was found that a higher spray flow rate does not necessarily lead to better cooling performance. Maintaining the flow within a reasonable range not only ensures an effective temperature and humidity distribution but also contributes to cost reduction and optimization of energy efficiency to a certain extent. These results contribute significantly to the ongoing development of sustainable and energy-efficient greenhouse technologies.

This study specifically examined the high-temperature conditions during the summer afternoons in Shanghai. While temperatures are lower during other times of the day, and the outdoor environment is less harsh, there is a possibility that these variations could affect the results. Therefore, we plan to extend the research in future work to explore a broader range of scenarios.

Statements and declarations.

Conflicts of Interest

The authors declare no conflicts of interest regarding the publication of this paper.

References

[1] Xu, Y., Li, X., Yang, Z., Li, H. and Gao, L. (2020) Analysis of the Reasons for the Gap between the Yield of Tomato Long Season Cultivation in China's Continuous Glass Greenhouse and That of the Netherlands. *China Vegetables*, No. 10, 1-8. https://d.wanfangdata.com.cn/periodical/ChlQZXJpb2RpY2FsQ0hJTmV3Uz-IwMjMxMjI2Eg16Z3NjMjAyMDEwMDAxGghvd2lwaGVraQ%3D%3D

[2] Shamshiri, R.R., Jones, J.W., Thorp, K.R., Ahmad, D., Man, H.C. and Taheri, S. (2018) Review of Optimum Temperature, Humidity, and Vapour Pressure Deficit for Microclimate Evaluation and Control in Greenhouse Cultivation of Tomato: A Review. *International Agrophysics*, **32**, 287-302. https://doi.org/10.1515/intag-2017-0005

[3] Sun, X., *et al.* (2021) Progress and Prospect of Research on Greenhouse Cooling Technology. *South China Agricultural*, **15**, 42-47.

[4] Li, Y., Wu, D. and Yu, Z. (1994) Simulation and Test Research of Micrometeorology Environment in a Sun-Light Greenhouse. *Transactions of the Chinese Society of Agricultural Engineering*, **10**, 130-136.

[5] Chen, Q. and Wang, Z. (1996) Dynamic Simulation of Sun-Light Greenhouse Thermal Environment. *Journal of China Agricultural University*, **1**, 67-72.

[6] Bai, J., Wen, X., Li, Y., Cui, J. and Ren, Y. (2019) Characteristics of Root Distribution and Water-Transportation Tissues of Apple Rootstocks Malusmicromaluand M9T337. *Journal of Shanxi Agricultural University*, **39**, 46-54.

[7] Han, Y., Li, A., Li, Y., Jia, X. and Zhao, D. (2015) The Influence of Different Root-zone Temperature Treatment on Tomato Leaves Stomata. *Journal of Shanxi Agricultural Sciences*, **43**, 1234-1236. https://kns.cnki.net/kcms2/article/abstract?v=ACks_bcdpKkLDhqym6jKdAcTgtRRacY2P4SWh-CXgksW_nAyASP_vR6EMmBP5hvv21963MgrFmVRILGUfCxl9uSwTh-eeL-bDS8C8rG4FK6vQc03q5bBCyATW8JmZxUAjDh9IFqJUUAyfBjBpzroUg==&uniplatform=NZKPT&language=CHS

[8] Yue, F., Huang, X. and Ji, Y. (2001) Study on Three-Dimensional and Efficient Planting Model of Strawberry and Muskmelon in Solar Greenhouse. *The Journal of Shandong Agricultural Administrators' College*, No. 3, 155-135.

[9] Li, C., Zhang, Y., Hu, Y., Lu, X. and Wang, X. (2009) Three-Dimensional Efficient Cultivation Pattern of Winter and Spring Stubble Solar Greenhouse Chilli-Bean Curd -Kale. *Agriculture Engineering Technology*, No. 2, 28-29.

[10] Okushima, L., Sase, S. and Nara, M. (1989) A Support System for Natural Ventilation Design of Greenhouses Based on Computational Aerodynamics. *Acta Horticulturae*, **248**, 129-136. https://doi.org/10.17660/actahortic.1989.248.13

[11] Molina-Aiz, F.D., Fatnassi, H., Boulard, T., Roy, J.C. and Valera, D.L. (2010) Comparison of Finite Element and Finite Volume Methods for Simulation of Natural Ventilation in Greenhouses. *Computers and Electronics in Agriculture*, **72**, 69-86. https://doi.org/10.1016/j.compag.2010.03.002

[12] Kang, L., Zhang, Y., Kacira, M. and van Hooff, T. (2024) CFD Simulation of Air Dis-

tributions in a Small Multi-Layer Vertical Farm: Impact of Computational and Physical Parameters. *Biosystems Engineering*, **243**, 148-174. https://doi.org/10.1016/j.biosystemseng.2024.05.004

[13] Saberian, A. and Sajadiye, S.M. (2019) The Effect of Dynamic Solar Heat Load on the Greenhouse Microclimate Using CFD Simulation. *Renewable Energy*, **138**, 722-737. https://doi.org/10.1016/j.renene.2019.01.108

[14] Xu, F., Lu, H., Chen, Z., Guan, Z., Chen, Y., Shen, G., *et al.* (2021) Selection of a Computational Fluid Dynamics (CFD) Model and Its Application to Greenhouse Pad-Fan Cooling (PFC) Systems. *Journal of Cleaner Production*, **302**, Article 127013. https://doi.org/10.1016/j.jclepro.2021.127013

[15] Benni, S., Tassinari, P., Bonora, F., Barbaresi, A. and Torreggiani, D. (2016) Efficacy of Greenhouse Natural Ventilation: Environmental Monitoring and CFD Simulations of a Study Case. *Energy and Buildings*, **125**, 276-286. https://doi.org/10.1016/j.enbuild.2016.05.014

[16] Xu, F., Cai, Y., Chen, J. and Zhang, L. (2015) Temperature/Flow Field Simulation and Parameter Optimal Design for Greenhouses with Fan-Pad Evaporative Cooling System. *Transactions of the Chinese Society of Agricultural Engineering*, **31**, 201-208.

[17] Shao, L. (2009) Numerical Analysis of Venlo-Type Greenhouse in Summer Thermal and Humid Environment. https://kns.cnki.net/kcms2/article/abstract?v=lWc4gvQ5J17QY_OvMGKAZRMcA12MenfTQ9d48ykVVjDJzM8S5uhXHgJdOAbCLZ0mFUhusCACBd5HCw2GhalCooYX6YuA-6usUGwtW3F2jCw-SoGOOkxqQAX2NqgKgFwaFr1qwas6Zulj941pV-louGA==&uniplatform=NZKPT&language=CHS

[18] He, X., Wang, J., Guo, S., Zhang, J., Wei, B., Sun, J., *et al.* (2018) Ventilation Optimization of Solar Greenhouse with Removable Back Walls Based on CFD. *Computers and Electronics in Agriculture*, **149**, 16-25. https://doi.org/10.1016/j.compag.2017.10.001

[19] Zhang, X., Wang, H., Zou, Z. and Wang, S. (2016) CFD and Weighted Entropy Based Simulation and Optimisation of Chinese Solar Greenhouse Temperature Distribution. *Biosystems Engineering*, **142**, 12-26. https://doi.org/10.1016/j.biosystemseng.2015.11.006

[20] Villagrán, E.A., Baeza Romero, E.J. and Bojacá, C.R. (2019) Transient CFD Analysis of the Natural Ventilation of Three Types of Greenhouses Used for Agricultural Production in a Tropical Mountain Climate. *Biosystems Engineering*, **188**, 288-304. https://doi.org/10.1016/j.biosystemseng.2019.10.026

[21] Roy, J.C., Vidal, C., Fargues, J. and Boulard, T. (2008) CFD Based Determination of Temperature and Humidity at Leaf Surface. *Computers and Electronics in Agriculture*, **61**, 201-212. https://doi.org/10.1016/j.compag.2007.11.007

[22] Ansys Fluent (2011) Ansys Fluent Theory Guide. Vol. 15317. Ansys Inc., 724-746.

[23] Aydogdu, M. (2023) Analysis of the Effect of Rigid Vegetation Patches on the Hydraulics of an Open Channel Flow with Realizable K-E and Reynolds Stress Turbulence Models. *Flow Measurement and Instrumentation*, **94**, Article 102477. https://doi.org/10.1016/j.flowmeasinst.2023.102477

[24] Salim, S.M. and Cheah, S. (2009) Wall Y+ Strategy for Dealing with Wall-Bounded Turbulent Flows. *Proceedings of the International Multiconference of Engineers and Computer Scientists*, **2**, 2165-2170.

[25] Lodh, B.K., Das, A.K. and Singh, N. (2017) Investigation of Turbulence for Wind

Flow over a Surface Mounted Cube Using Wall Y+ Approach. *Indian Journal of Science and Technology*, **10**, 1-11. https://doi.org/10.17485/ijst/2017/v10i8/109197

[26] Zhang, X. (2021) How to Cool Down Vegetable Greenhouses in Summer. *The Farmers Consultant*, No. 19, 48-49. https://d.wanfangdata.com.cn/periodical/ChlQZXJpb2RpY2FsQ0hJTmV3Uz-IwMjMxMjI2Eg1uamNtMjAyMTE5MDQ1Ggh0N3ZqOGxwdA%3D%3D https://doi.org/10.23880/chij-16000125

[27] Kong, D., Yu, H., Li, Y. and Tian, Y. (2010) Effect of Drought Stress on Photosynthesis and Physiologica Characteristics of Chrysanthemum Morifolium. *Journal of Northwest A & F University-Natural Science Edition*, **38**, 103-108.

[28] Chacón-Rebollo, T. and Lewandowski, R. (2013) Mathematical and Numerical Foundations of Turbulence Models and Applications. Birkhäuser New York.

[29] Chang, W. (2023) Experimental and Numerical Study on Precise Spray Ventilation Cooling and Humidity Control in Greenhouse. https://link.cnki.net/doi/10.27012/d.cnki.gdhuu.2023.001142

[30] Liu, F. and Weng, M. (2021) Experimental Design and Data Processing. Chongqing University Press, Chongqing

[31] Wang, M., Zhao, T., Zhang, W. and Shi, Y. (2007) Effects of Interactions between Elevated CO_2 Concentration and Temperature Drought on Physio-Ecological Processes of Plants. *Agricultural Research in the Arid Areas*, No. 2, 99-103. https://kns.cnki.net/kcms2/article/abstract?v=vYzgd5_tBo8GtG-Su-_G_sbb1KfcZAVW2--N5qENopTCkPC_m0TX8aJsBIYXsblV-5A5yVISvh-DOeb5q2M3mAsQSjMDbL7Ds9z_pzBz0iSFhzj6SLBvgXGllB3JLp5rGyH79Wa5KAE=&uniplatform=NZKPT&language=CHS

[32] Liu, Y. and Ding, J. (2007) Effect of Temperature and Humidity on Chrysanthemum Seedlings. *Modern Agriculture*, No. 11, 14-17.